Effect of electric potential structures on Jovian S-burst morphology

Sébastien L. G. Hess, Fabrice Mottez, Philippe Zarka

▶ **To cite this version:**

Sébastien L. G. Hess, Fabrice Mottez, Philippe Zarka. Effect of electric potential structures on Jovian S-burst morphology. Geophysical Research Letters, 2009, 36, pp.14101. 10.1029/2009GL039084 . hal-03786209

HAL Id: hal-03786209
https://hal.science/hal-03786209v1

Submitted on 24 Sep 2022

HAL is a multi-disciplinary open access archive for the deposit and dissemination of scientific research documents, whether they are published or not. The documents may come from teaching and research institutions in France or abroad, or from public or private research centers.

L'archive ouverte pluridisciplinaire **HAL**, est destinée au dépôt et à la diffusion de documents scientifiques de niveau recherche, publiés ou non, émanant des établissements d'enseignement et de recherche français ou étrangers, des laboratoires publics ou privés.

Copyright

Effect of electric potential structures on Jovian S-burst morphology

S. Hess,[1,2,3] F. Mottez,[1] and P. Zarka[2]

Received 7 May 2009; revised 9 June 2009; accepted 16 June 2009; published 16 July 2009.

[1] Jupiter's radio emissions are dominated in intensity by decametric radio emissions due to the Io-Jupiter interaction. A significant part of these emissions consists of short radio bursts (so-called S-bursts) drifting in time and frequency. Previous analyses suggest that these emissions are cyclotron-maser emissions in the flux tube connecting Io or Io's wake to Jupiter. We present simulations of these electrons under the assumption of acceleration by Alfvén waves in the Io flux tube. Near Jupiter, a loss cone and a ring distribution appear in the magnetically mirrored electron population, which can then amplify extraordinary (X) mode radio waves. The X-mode growth rate is computed, which allows us to build theoretical dynamic spectra of the resulting Jovian radio emissions. Additional potential structures are assumed in the Jovian auroral region. We reconstruct their impact on the morphology of the emission. They match some of the time-frequency patterns observed with Jovian S-bursts. This provides the first evidence of bipolar electrostatic structures in the Jovian auroral region. **Citation:** Hess, S., F. Mottez, and P. Zarka (2009), Effect of electric potential structures on Jovian S-burst morphology, *Geophys. Res. Lett.*, *36*, L14101, doi:10.1029/2009GL039084.

1. Introduction

[2] The motion of the satellite Io across Jovian magnetic field lines in the plasma torus surrounding its orbit provides an important and continuous energy source for electron acceleration, ultimately generating bright auroral spots at the Io flux tube (IFT) footprint [*Connerney et al.*, 1993] and intense decametric radio emissions [*Queinnec and Zarka*, 1998]. The electric field generated by this motion is thought to induce electric currents and/or Alfvén waves [*Goldreich and Lynden-Bell*, 1969; *Neubauer*, 1980] which may both accelerate electrons in the plasma torus and in the Io flux tube (IFT). Due to the magnetic mirror effect near the Jovian ionosphere, these electrons acquire an unstable distribution relative to the Cyclotron-Maser Instability (CMI) [*Wu*, 1985].

[3] We assume that the CMI is responsible for the emissions since it is observed in many auroral contexts, in particular that of the auroral kilometric radiation. A more developed discussion is given by *Zarka* [1998] which justifies our choice.

[4] Millisecond (or S-) bursts are discrete and intense emissions occurring near the electron cyclotron frequency and drifting in the frequency-time plane. Figure 1 (top) shows a typical dynamic spectrum of these emissions. Their sources propagate like electrons in quasi-adiabatic motion moving along the magnetic field lines away from Jupiter [*Ellis*, 1965; *Hess et al.*, 2007a, and references therein]. Burst occurrence seems often quasi-periodic with a rate of the order of 10 Hz. The quasi-periodic, discrete nature of the S-bursts, originating from a continuous excitation, has been investigated by *Hess et al.* [2007b]. The authors proposed that Alfvén waves (AW) could accelerate electrons periodically and thus produce periodic bursts.

[5] The electron acceleration by Alfvén waves was simulated along the Io Flux Tube (IFT) and the CMI growth rates deduced from the electron distribution. The time/frequency evolution of the maximal value of the growth rate matches well the dynamic spectra recorded from the ground (Figure 1, bottom). Thus *Hess et al.* [2007b] concluded that the electron acceleration by Alfvén waves is the main process generating the Jovian S-bursts.

[6] This result is only a first order approximation that does not cover the whole range of the S-burst morphologies and the large variety of processes which occur in the Jovian auroral regions.

[7] A classification of the S-burst morphologies has been performed by *Riihimaa* [1991], who defined ~20 different shapes of S-bursts, with only two of them corresponding to the typical, adiabatic, shape. Most are mainly characterized by a strong perturbation of the S-burst slope on a narrow frequency range. Some S-bursts with complex morphology are shown in Figures 2a, 2b, and 2c. Moreover the S-bursts are often associated with narrowband emission (so-called N-bursts) with which they seem to interact [*Riihimaa*, 1991].

[8] *Hess et al.* [2007a, 2009], have shown from experimental data the presence of potential jumps of few 100's eV, located at altitudes around 0.1 R_J, which move at the local sound velocity along the magnetic field lines. These potential jumps are not the primary source of electron acceleration as an energy of several keV is needed. But being located below the AW electron acceleration region (0.9 R_J in altitude), they create a supplementary downward acceleration. We are here interested in the perturbation of the typical S-burst shape induced by the presence of additional electric potential structures in the emission region.

[9] We use a particle test code to compute particles motion along the IFT (section 2.1). The introduction of Alfvén waves is discussed in section 2.2 and CMI growth rate computations in section 2.3. S-burst shapes resulting from additional introduction of potential structures are presented in section 3 and discussed in section 4.

2. Description of the Simulation Code

[10] The code used in the present study is the same than that of *Hess et al.* [2007b]. A more detailed description of the code can be found in that paper.

[1]LUTH, Observatoire de Paris, CNRS, Meudon, France.
[2]LESIA, Observatoire de Paris, CNRS, Meudon, France.
[3]Now at LASP, University of Colorado, Boulder, Colorado, USA.

Copyright 2009 by the American Geophysical Union.
0094-8276/09/2009GL039084

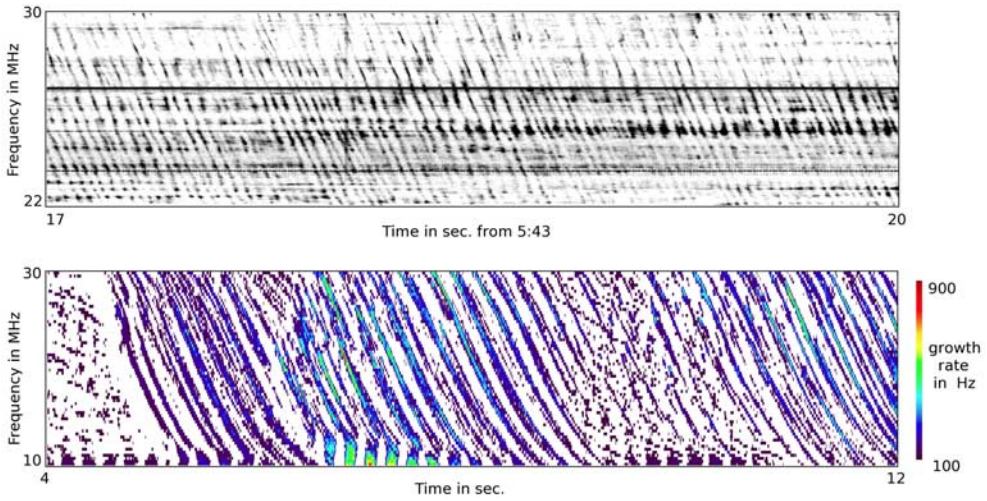

Figure 1. (top) Dynamic spectrum recorded at the Nançay decameter array in April 1995. The drifting structures are Jovian S-bursts. They show a negative drift rate of about −20 MHz/s, corresponding to the anti-planetward adiabatic motion of the emitting electrons. (bottom) Dynamic spectrum of the CMI growth rates for a simulation with an acceleration by Alfvén wave and without any additional electric potential structures. The dynamic spectrum shows S-bursts with a typical shape (to compare with Figure 1a). The quasi-periodicity in both plots results from the Alfvén wave period [*Hess et al.*, 2007b]. The time scale of the two dynamic spectra is different due to the fact that our simulation code is unable to simulate Alfvén waves with the frequency observed in the S-burst dynamic spectrum. The observed dynamic spectrum is cut at 22 MHz since there is no observed emission at lower frequency (probably due to visibility effects).

2.1. Particle Motion and Injection

[11] We simulate the motion of electron guiding-centers in imposed (not self-consistent) electromagnetic and gravitational fields. We simulate only the hot component of Io's electron population, which thermal velocity is about 200 eV as measured by the instruments onboard Voyager and Galileo [*Moncuquet et al.*, 2002]. A constant flux of particles (∼700 at each time step) is injected at the Io boundary. The particles can exit the simulation at both ends of the grid. Our simulation is made with 6.4×10^7 particles on a 4096 cells grid. The length of a grid cell is $\Delta x = 114$ km $\simeq 1.16 \times 10^{-3}\ R_J$, therefore, the total length of the system is $L = N\Delta x = 6.5\ R_J$, i.e., the length of the magnetic field lines from Io to Jupiter.

[12] The equation of motion is given by the conservation of the magnetic moment μ and by the gradients of the electric potential ϕ_E and the gravitational (and inertial) potential ϕ_G.

$$\mu = v_\perp^2/B = const. \tag{1}$$

$$\frac{dv_\parallel}{dt} = -\nabla\left(\frac{q}{m}\phi_E + \mu B + \phi_G\right) \tag{2}$$

The permanent magnetic field is computed using the VIP4 multipolar magnetic model of Jupiter [*Connerney et al.*, 1998], built from in-situ magnetic field measurements of Voyager and Pioneer, and from infrared observations of the position of the IFT footprints on Jupiter. Up to now, this is the most accurate published model for the computation of the magnetic field along the IFT. We choose here to simulate the magnetic field line in the northern hemisphere whose longitude at equator is 230°. It corresponds to the mid-point of the range of longitudes active in radio [*Carr et al.*, 1983; *Queinnec and Zarka*, 1998].

[13] The gravitational (and inertial) potential ϕ_G is given by the Jovian attraction and the centrifugal potential. Io's attraction is neglected. We estimate the ambipolar electric potential ϕ_E resulting from the gradient of the gravitational potential ϕ_G only.

2.2. Alfvén Waves

[14] In ideal MHD, Alfvén waves have a wave length $\lambda \gg \rho_s$ and $\lambda \gg \lambda_e$ where ρ_s is the ion acoustic gyroradius and λ_e is the electron skin depth, and they carry only a perpendicular electric field. Thus they cannot accelerate electrons. In the case of shorter wavelength, the kinetic Alfvén wave theory [*Lysak and Song*, 2003] shows that the Alfvén waves can carry a parallel electric field.

$$\delta E_\parallel \simeq \omega_a k_\perp \lambda_e^2 \delta B_\perp \tag{3}$$

where ω_a is the Alfvén wave frequency. The perpendicular wavelength $\lambda_\perp$ is proportional to the flux tube section (i.e., to $B^{1/2}$) with a value of ∼10 *km* at the Jovian surface in our simulation. We introduce near Io's torus border (1.6 R_J from Io) a planetward Alfvén waves train during 10 seconds with a frequency of 5 Hz. This frequency is chosen because our code resolution do not allow to simulate the 15 Hz mean frequency of the real S-bursts. Such short wavelength, high frequency, waves are observed near Io (with amplitudes of ∼10 nT) and are thought to be due to the filamentation of long-scale waves in the torus [*Chust et al.*, 2005].

[15] An Alfvén wave amplitude ≥100 nT appears to be necessary to generate an electric field strong enough to

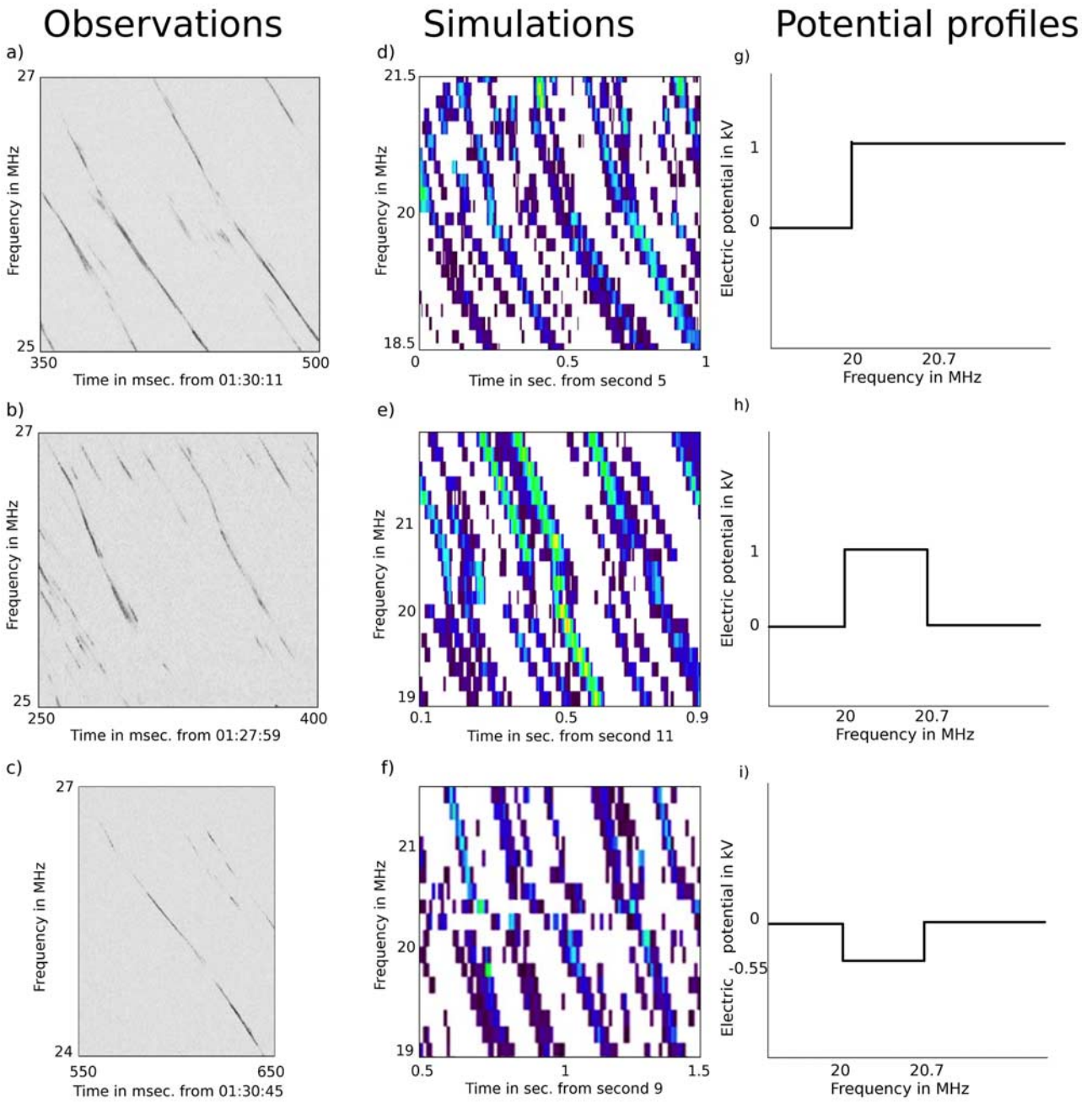

Figure 2. (a, b, and c) Dynamic spectra of S-bursts with non typical shapes recorded at UTR-2 Kharkov telescope on March 14, 2005. (d) Simulated dynamic spectrum of an S-burst emission with a 1 kV potential jump at an altitude corresponding to a gyrofrequency of 20 MHz (g), which reproduces well the observed dynamic spectrum (Figure 2a). (e) Simulated dynamic spectrum of an S-burst emission with a 1 kV potential enhancement at an altitude corresponding to gyrofrequencies between 20 and 20.7 MHz (h), it reproduces well the observed dynamic spectrum (Figure 2b). (f) Simulated dynamic spectrum of an S-burst emission with a 550 V potential drop-off at an altitude corresponding to gyrofrequencies between 20 and 20.7 MHz (i), which reproduces well the observed dynamic spectrum (Figure 2c). The color scale is the same as for Figure 1.

accelerate the electrons to an energy of a few keV, but is larger than what is expected for such short waves. However the ionospheric feedback coupled to a ionospheric resonance can amplify waves near 10–20 Hz, allowing such amplitudes [*Su et al.*, 2006, and references therein].

[16] The wave introduced in our simulations has an amplitude of ~250 nT which generates bursts thin enough so we can see clearly the variations of their slopes (probably an effect of the limited resolution of our code). As our simulation scheme does not allow for self-consistent electromagnetic fields, the Alfvén wave propagation along the

field lines and their associated parallel electric fields (equation (3)) are computed analytically, taking into account the density and magnetic field intensity variations.

2.3. Cyclotron-Maser Growth Rate

[17] A complete description of the linear Cyclotron Maser Instability (CMI) theory is presented by *Wu* [1985]. CMI occurs for electrons which fulfill the wave-particle resonance condition:

$$\omega = \omega_c/\Gamma + k_{\|} v_{\|} \tag{4}$$

where ω is the wave frequency, ω_c the electron cyclotron frequency and Γ the relativistic Lorentz factor. In the weakly relativistic approximation the wave-particle resonance condition is represented by a circle in the ($v_{\|}$, $v_{\perp}$) plane of center v_0 and vector-radius **R** given by

$$\mathbf{v}_0 = c\frac{\mathbf{k}.\mathbf{b}}{k} \simeq \frac{k_{\|}c^2}{\omega_c}\mathbf{u}_{\|} \quad ; \quad R = \sqrt{v_0^2 - 2\left(\frac{\omega}{\omega_c} - 1\right)}, \tag{5}$$

where **b** and $\mathbf{u}_{\|}$ are the unit vectors of the magnetic field and of the parallel velocity. The maser cyclotron growth rate γ is obtained by integration over the resonance circle of the gradient of the particle distribution $f(\mathbf{v}_0, \mathbf{R})$ relative to the perpendicular velocity. Positive growth rates require positive integrated gradients [*Wu*, 1985]. In our simulation we compute the growth rates from the particle distributions along the field line for several resonance circle centers v_0 and radii R. Each of them corresponds to an extraordinary mode (characterized by a frequency ω and a parallel wave vector $k_{\|}$), the most amplified mode dominates the instability (in the linear approximation) and may thus be observed. Therefore we retain the mode with the largest growth rate. The modes whose growth rates are computed in our study are those for which:

$$k_{\|} = \frac{v}{c^2}\frac{\omega_c}{\cos\alpha} \quad ; \quad \omega = \omega_c\left(1 + \frac{v^2}{c^2}\right) \tag{6}$$

where $\alpha = \arccos(v_{\|}/v)$ is the resonant particle pitch angle. These modes correspond to those that trigger the S-burst emission in the simulations of *Hess et al.* [2007b]. A discussion of the validity of this choice can be found in that paper.

3. Simulations and Results

[18] We start from the simulation of *Hess et al.* [2007b], which consists in an acceleration of the electrons by an Alfvén wave, without adding any electric potential structures. The result of this simulation is shown in Figure 1 (bottom), where the computed CMI growth rate is plotted versus frequency and time. The growth rate values are given above a background value of ~200 Hz which is due to the permanent loss-cone distribution of the electrons. The typical shape of the S-bursts, due to the adiabatic motion of anti-planetward electrons, is well reproduced. The mean drift rate is ~20 MHz/s, consistent with observations. In our study we are interested by the perturbation of this typical shape induced by the presence of additional electric potential structures in the emission region. We simulate three kinds of potential structures: the potential jumps discovered by *Hess et al.* [2007a], which are localized (less than few hundreds of kilometers wide), with an amplitude up to 1.5 kV; and the bipolar electrostatic structures (with both polarizations), which are commonly observed in the terrestrial auroral region. The latter two structures are here modeled by two consecutive potential jumps with opposite polarities. The simulation results are compared to observations made at the Kharkov UTR-2 telescope on March 14, 2005, which are the cleanest observations we have. This day most of the potential structures were observed near a frequency of 26 MHz. Due to the limited resolution of our code we did not simulate potential structures at this frequency (too strong magnetic field gradients), but between 20 and 20.7 MHz (~0.14–0.15 R_J from the Jovian ionosphere). Moreover we used large potential drop amplitudes (up to 1 kV) to balance the low resolution and to enhance the effect of such a potential structure on the S-burst shape. The perturbations of the burst slope due to lower values of the amplitude may be difficult to detect. However we are here only interested by reproducing qualitatively the shape variations (mainly breaks in slope) introduced by potential structures and not by reproducing exactly a given burst.

3.1. Potential Jumps

[19] We reproduce the simulation of electron acceleration by Alfvén waves with a supplementary electric potential jump, with a 1kV amplitude, at an altitude corresponding to a local electron gyrofrequency (f_{ce}) of 20 MHz. The electric field polarization is set to accelerate the electrons toward Jupiter, consistently with the observations of electric potential jumps made by *Hess et al.* [2007a].

[20] This potential jump induces a sharp variation of the electron velocity, which appears on the growth rate dynamic spectrum as a sharp variation of the S-burst slope. Figure 2d shows a zoom of the resulting dynamic spectrum, centered on the potential jump position. The break in the S-burst slope is visible at f_{ce} = 20 MHz.

[21] Figure 2a shows a typical example of bursts which exhibit the same shape (break in slope) as those simulated. A study of the S-burst drift, similar to those performed by *Hess et al.* [2007a] was done, which indeed reveals the presence of a potential jump at $f_{ce} \sim$ 26 MHz [*Hess et al.*, 2009].

3.2. Potential Enhancement

[22] We perform a simulation with two potential jumps of opposite polarities, one located at an altitude corresponding to f_{ce} = 20 MHz which accelerates the electron toward Jupiter and the other at an altitude corresponding to $f_{ce} \sim$ 20.7 MHz which accelerates the electrons in the opposite direction. Both potential jumps have a 1 kV amplitude.

[23] The resulting perturbation of the S-burst shape is shown on Figure 2e. Inside the potential enhancement the S-burst drift rate reaches higher value than outside (the bursts seems nearly vertical). This kind of perturbation is seen in the observations (Figure 2b), implying that such bipolar electrostatic structures are present in the Jovian auroral region.

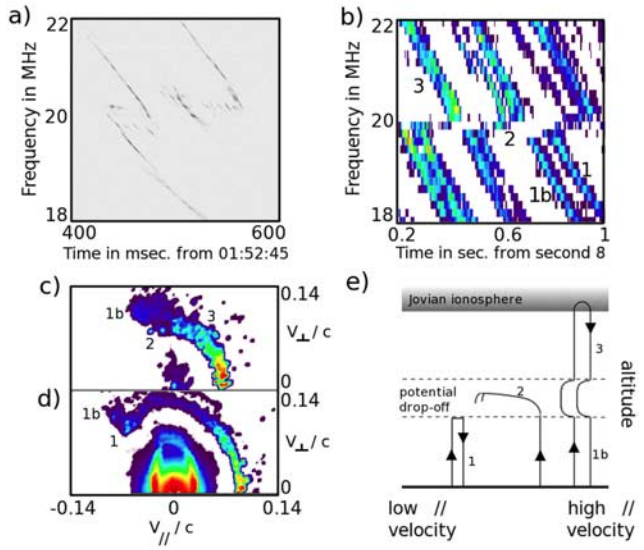

Figure 3. (a) Dynamic spectrum showing the interaction between the S-bursts (oblique) and the N-bursts (horizontal). (b) Simulated dynamic spectrum with a 800V potential drop-off (20–20.2 MHz). The bursts present 4 components: 1, 1b low frequency S-bursts, 2 narrow band emission, 3 high frequency S-bursts. (c) Electron distribution at an altitude at which f_{ce} = 20.1 MHz. (d) Electron distribution at an altitude at which f_{ce} = 19.6 MHz. (e) Sketch of the passing and reflected trajectories of the electrons in the S-bursts emission region. The color scale is the same as for Figure 1.

3.3. Potential Drop-off

[24] Another simulation is done with two potential jumps, located at the same altitude as for the potential enhancement, but with opposite polarities, thus modelizing a potential drop-off. The electrons are decelerated when approaching the structure. We set the potential jump to an amplitude of 550 V in order to keep it significantly below the parallel energy of the emitting electron (~1 keV).

[25] As compared to the previous case, the presence of the potential drop-off affects the electron velocity (and thus the S-burst slope) in an opposite way (the slope is lower in absolute value within the structure). The result of the simulation is shown in Figure 2f. Figure 2c shows an observed S-burst dynamic spectrum for which the S-burst shape is consistent with the presence of a such a potential drop-off.

[26] When the electric potential jumps amplitude approaches the parallel kinetic energy of the electrons, the shape of the simulated bursts changes. Figure 3b shows the result for a potential drop-off located between 20 MHz and ~20.2 MHz whose amplitude is 800 V. The bursts are then divided into 4 components: two low frequency S-bursts (1 and 1b), a narrow band part (2) and a high frequency S-burst (3). It is due to the division of the planetward electron beam distribution (Figures 3c and 3d) into a part reflected by the low frequency potential jump (1), a part reflect in the potential structure by magnetic mirroring (2) and a passing part, generating a normal S-burst (3 and 1b). A faint secondary burst is often seen in the high-frequency range which is due to secondary reflections. The time-frequency emission structure seems comparable to the S- and N-bursts interaction (Figure 3a).

4. Conclusion

[27] By adding electric potential structures in the emission region (at an altitude of ~0.15 R_J) we are able to reproduce many of the S-burst shapes described by *Riihimaa* [1991], since most of them are parts of the complete S-bursts we simulate. These shapes present one or two breaks in the S-bursts slope, which correspond to a modification of the emitting electron energy induced by the presence of the potential jumps. However, we are not able to generate the narrow band (N-bursts) emission associated to S-bursts with potential jump amplitudes lower than several (4–5) times the typical thermal energy of the hot electrons (~200 eV). The N- and S-bursts interaction may thus involve other process(es), or successive potential jumps.

[28] The present study shows that the existence of non-typical shapes of the S-bursts is fully consistent with the standard scenario of S-burst generation: electron beams in adiabatic motion (outside of localized electric potential structures) [*Ellis*, 1965; *Hess et al.*, 2007a] and accelerated by Alfvén waves [*Hess et al.*, 2007b]. *Hess et al.* [2007a] observed that the emission region can host many regions in which the electron motion is adiabatic separated by potential jump. Here we also found localized (weak) perturbations of the emitting electron energy within an adiabatic region.

References

Carr, T. D., M. D. Desch, and J. K. Alexander (1983), Phenomenology of magnetospheric radio emissions, in *Physics of the Jovian Magnetosphere*, edited by A. J. Dessler, pp. 226–284, Cambridge Univ. Press, Cambridge, U. K.

Chust, T., A. Roux, W. S. Kurth, D. A. Gurnett, M. G. Kivelson, and K. K. Khurana (2005), Are Io's Alfvén wings filamented? Galileo observations, *Planet. Space Sci.*, *53*, 395–412, doi:10.1016/j.pss.2004.09.021.

Connerney, J. E. P., R. Baron, T. Satoh, and T. Owen (1993), Images of excited H_3^+ at the foot of the Io flux tube in Jupiter's atmosphere, *Science*, *262*, 1035–1038, doi:10.1126/science.262.5136.1035.

Connerney, J. E. P., M. H. Acuña, N. F. Ness, and T. Satoh (1998), New models of Jupiter's magnetic field constrained by the Io flux tube footprint, *J. Geophys. Res.*, *103*, 11,929–11,940.

Ellis, G. R. A. (1965), The decametric radio emission of Jupiter, *Radio Sci.*, *4*, 1513–1530.

Goldreich, P., and D. Lynden-Bell (1969), Io, a Jovian unipolar inductor, *Astrophys. J.*, *156*, 59–78.

Hess, S., P. Zarka, and F. Mottez (2007a), Io-Jupiter interaction, millisecond bursts and field-aligned potentials, *Planet. Space Sci.*, *55*, 89–99.

Hess, S., F. Mottez, and P. Zarka (2007b), Jovian S burst generation by Alfvén waves, *J. Geophys. Res.*, *112*, A11212, doi:10.1029/2006JA012191.

Hess, S., P. Zarka, F. Mottez, and V. B. Ryabov (2009), Electric potential jumps in the Io-Jupiter flux tube, *Planet. Space Sci.*, *57*, 23–33.

Lysak, R. L., and Y. Song (2003), Kinetic theory of the Alfvén wave acceleration of auroral electrons, *J. Geophys. Res.*, *108*(A4), 8005, doi:10.1029/2002JA009406.

Moncuquet, M., F. Bagenal, and N. Meyer-Vernet (2002), Latitudinal structure of outer Io plasma torus, *J. Geophys. Res.*, *107*(A9), 1260, doi:10.1029/2001JA900124.

Neubauer, F. M. (1980), Nonlinear standing Alfvén wave current system at Io: Theory, *J. Geophys. Res.*, *85*, 1171–1178.

Queinnec, J., and P. Zarka (1998), Io-controlled decameter arcs and Io-Jupiter interaction, *J. Geophys. Res.*, *103*, 26,649–26,666.

Riihimaa, J. J. (1991), Evolution of the spectral fine structure of Jupiter's decametric S-storms, *Earth Moon Planets*, *53*, 157–182.

Su, Y.-J., S. T. Jones, R. E. Ergun, F. Bagenal, S. E. Parker, P. A. Delamere, and R. L. Lysak (2006), Io-Jupiter interaction: Alfvén wave propagation and ionospheric Alfvén resonator, *J. Geophys. Res.*, *111*, A06211, doi:10.1029/2005JA011252.

Wu, C. S. (1985), Kinetic cyclotron and synchrotron maser instabilities: Radio emission processes by direct amplification of radiation, *Space Sci. Rev.*, *41*, 215–298.

Zarka, P. (1998), Auroral radio emissions at the outer planets: Observations and theories, *J. Geophys. Res.*, *103*, 20,159–20,194.

S. Hess, LASP, University of Colorado, 1234 Innovation Drive, Boulder, CO 80303, USA.

F. Mottez, LUTH, Observatoire de Paris, CNRS, 5 place Jules Janssen, F-92195 Meudon CEDEX, France.

P. Zarka, LESIA, Observatoire de Paris, CNRS, 5 place Jules Janssen, F-92190 Meudon CEDEX, France. (philippe.zarka@obspm.fr)